ISSN 1070-4272, Russian Journal of Applied Chemistry, 2015, Vol. 88, No. 10, pp. 1711−1717. © Pleiades Publishing, Ltd., 2015.

VARIOUS TECHNOLOGICAL PROCESSES

Electrochemical Performance of γMnO_2 Prepared from the Active Mass of Used Batteries[1]

K. Noufel[a]*, A. Bouzid[a], N. Chelali[a], and L. Zerroual[b]

[a] *Laboratoire Matériaux et Systèmes Electroniques (LMSE), Faculté des Sciences et Technologie, Université de B.B. Arreridj-Route d'El Annasser, 34000, Algérie*
[b] *Laboratoire d'Energétique et D'électrochimie du solide, Université de Sétif-1, Sétif 19000, Algérie*
e-mail: kamelnoufel@yahoo.fr

Received September 18, 2015

Abstract—We prepared MnO_2 by electrolysis of manganese sulfate solution recovered from used batteries and commercial manganese sulfate solution. The comparative study of the two samples using electrochemical techniques in alkaline solution shows that the two samples exhibit the same behavior. From XRD, we identified and indexed both samples by γMnO_2 orthorhombic structure. We estimated the proton diffusion coefficient using galvanostatic intermittent titration technique (GITT). Our calculated data are in good agreement with theoretical values for both samples. In addition TG analysis shows the same thermal profile for both samples.

DOI: 10.1134/S1070427215100249

INTRODUCTION

Batteries represent in term of heavy metal an important environmental pollutant [1], and are used in electronic devices as cellular phones, computers and video recorder. The development of recycling batteries [2−4] processes is convenient for economic and environmental reasons such as high coast, waste recycling and natural resources conservation. Various methods were developed to recover used batteries, in particular, pyrometallurgical and hydrometallurgical processes [5−8]. Comparatively with the thermal process, the hydrometallurgical and electrochemical processes are complete recovery of metal with high purity, low energy requirement, avoidance of air emissions and minimization of waste water [9−12]. For the hydrometallurgical treatment of spent batteries, the solid material is mostly leached and dissolved in acid medium such as nitric acid, sulfuric acid or their mixtures [5−8]. Then, it is processed to recover the metal ions. The experimental approach used in this study is to produce leach liquor from saline and alkaline Leclanchй cells to obtain the $MnSO_4$ solutions Manganese dioxide exists in different allotropic crystallographic varieties. It is the main compound of the cathode of saline and alkaline Leclanché cells [13]. The cathode of these cells, consists generally of a mixture of chemical and electrochemical γMnO_2 in different proportion depending on the companies recipes and formula. Once discharged these cells still contain active γMnO_2.

The main purpose of this work consists of the elaboration of new materials from piles users and environmental protection from special waste and to recover manganese dioxide from used batteries. The material is chemically converted to Mn^{2+} solution [14, 15] then crystallized as manganese sulfate salt [16]. Finally γMnO_2 is prepared by electrolysis of $MnSO_4$ solutions. The different samples were characterized by X-ray diffraction analysis to determine the phase composition, the structure, the texture, the lattice parameters and the grains size. The electrochemical activity of γMnO_2 is compared to that obtained from Prolabo product $MnSo_4$ solution in the same conditions in alkaline medium. Linear sweep voltametry, galvanostatic discharge and impedance spectroscopy were used as techniques of investigation. The value of diffusion coefficient of proton [17, 18] is estimated by the Galvanostatic Intermittent Titration Technique (GITT) [19].

[1] The text was submitted by the authors in English.

EXPERIMENTAL

Sample Preparation

The active mass is recovered from used batteries. It is washed in running water to dissolve the salts and to eliminate carbon black. Let us that the carbon black in aqueous solution, where the density is 0.015, fleet on-surface and he is eliminated by simple scraping. It is filtered and overnight dried in an oven 8 g of MnO_2 powder is added to 1.5 g of oxalic acid with 15 mL of 98% sulfuric acid solution. The mixture is stirred and heated during five min, 50 mL of distilled water were then poured. After cooling we obtain a solution of $MnSO_4$ from the reaction [1, 20]:

$$MnO_2 + H_2SO_4 + C_2H_2O_4 \rightarrow MnSO_4 + 2CO_2 + H_2O.$$

This solution is crystallized to obtain a light pink $MnSO_4$ powder. γMnO_2 thin films were electrochemically deposited on Platinum electrode from $MnSO_4$ solution using the method described in the litterature [21]. γMnO_2 was also deposited in the same conditions from Prolabo $MnSO_4$. Thin films of γMnO_2 were deposited from $MnSO_4$ solutions under an anodic current of 0.5 A during three minutes on Platinum electrode with a surface area of 0.5 cm^2 at a temperature of 85°C. Then we study the electroactivity of manganese dioxide according to the fellowing reactions:

$$\text{Anode reaction } MnSO_4 + 2H_2O \rightarrow MnO_2 + H_2SO_4 + 2e + 2H^+,$$

$$\text{Cathode reaction } 2H^+ + 2e \rightarrow H_2.$$

$$\text{Global reaction } MnSO_4 + 2H_2O \rightarrow MnO_2 + H_2SO_4 + 2H^+.$$

We adopt the notation $(\gamma MnO_2)_R$ for the sample prepared from crystallized $MnSO_4$ prepared from the active material of used batteries and $(\gamma MnO_2)_L$ for the sample deposited from solution of $MnSO_4$ purchased from Prolabo product.

X-ray Diffraction Analysis

-1Bruker D8 advance diffractometer operating at 40 kV and 30 mA with CuK radiation (λ = 0.15406 nm). Radial scans were recorded in the reflection scanning mode with 2θ being changed from 10 to 90°C. Bragg's law, defined as $2d\sin\theta = n\lambda$, was used to compute the crystallographic distance (d_{hkl}) for the examined MnO_2 samples. The average crystallite size D was calculated from the full width at the half maximum (FWHM) of lines using Sherrer equation. [011] diffraction

Thermal Analysis

Thermogravimetric analysis (TGA tests were performed using instruments supplied by Metler Toledo: TGA/SDTA 851e. All measurements were carried out in air at a constant heating rate of 5 K min^{-1}. The samples were dried at 60°C to evaporate the surface absorbed water.

Electrochemical Tests

The electrochemical tests namely linear sweep voltametry, galvanostatic discharge, galvanostatic intermittent titration curves and impedance spectroscopy plots were carried out at room temperature using a Voltalab 40 PGZ 301 potentiostat-galvanostat, and a thermostated three-electrode cell. In all experiments the working electrode is a Platinum foil of surface area of 0.5 cm^2. The counter electrode is a carbon bar, the reference is Hg/HgO electrode. The electrolyte is a solution of 1 M KOH.

Linear sweep voltametry of the two samples $(\gamma MnO_2)_R$ and $(\gamma MnO_2)_L$ as conducted at a scan rate of 5 mV s^{-1} in a range of potential varying from 0.2 to –0.6 V. The potential at open circuit for the two samples is 0.2 V. Discharge tests were performed at a constant current of 30 μA and the curves $E = f(t)$ were recorded. Intermittent galvanostatic discharges were carried out in the same conditions by applying a current of 50 μA during 1 mn in each sequence, then the current was switched off and the cell was left to relax. The curves $E_{i=0} = f(x)$ were recorded.

Impedance measurements were performed in the frequency range from 100 mHz to 10 kHz at a signal amplitude of 10 mV. Impedance spectra were recorded at open circuit potential.

RESULTS AND DISCUSSION

Structural Properties

The XRD spectra have been used to determine the texture, the lattice parameter and the grain size for the two samples of MnO_2 as shown in Fig. 1. All detected peaks were identified to be γMnO_2 with orthorhombic structure. The appeared peaks in the spectra were identified as the (110), (210), (011), (211), (221), and (421) peaks of the γMnO_2 orthorhombic structure with a preferred texture of (011) . Moreover, from the X-ray spectra of (γMnO_2)

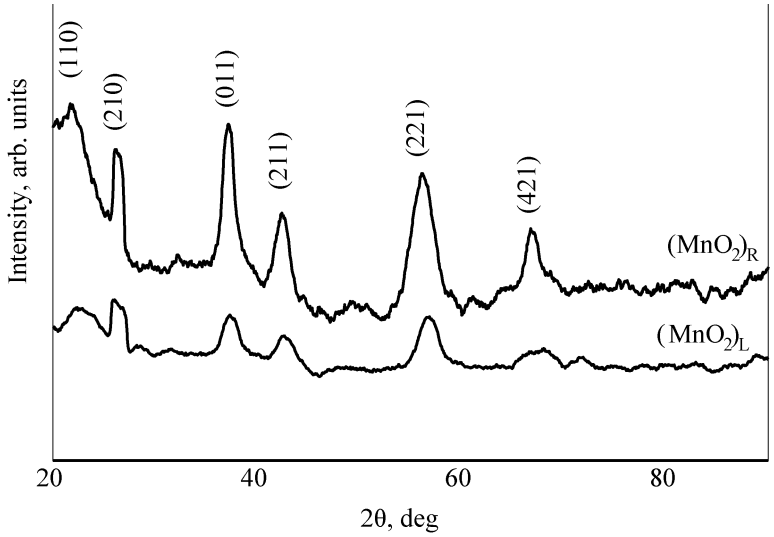

Fig. 1. X-ray diffraction spectra for $(\gamma MnO_2)_R$ and $(\gamma MnO_2)_L$ samples.

$_L$ and $(\gamma MnO_2)_R$, we derived the lattice constants *a*, *b* and *c* as well by the following equation:

$$\frac{1}{\sqrt{\frac{h^2}{a^2}+\frac{k^2}{b^2}+\frac{l^2}{c^2}}}=\frac{\lambda}{2\sin\theta}. \quad (1)$$

The computed values of *a*, *b* and *c* for different crystallographic orientations are reported in Table 1. These lattice parameters are in good agreement with the bulk value ones (*a* = 0.93229 nm, *b* = 0.44533 nm, and *c* = 0.28482 nm) cited in the literature [22].

Furthermore, we have also computed the grain sizes using the X-ray diffraction patterns and the Scherer formula [23]:

$$D=\frac{\lambda}{\Delta\theta\cos\theta}, \quad (2)$$

where *D* is the grain size for a grain with a particular texture (011) , λ the X-ray wavelength, θ the diffraction angle and Δθ the width at half height of the Bragg peak corresponding to this particular orientation. The grain size values of $(\gamma MnO_2)_L$ and $(\gamma MnO_2)_R$ are shown in Table 1. From these data we deduced that the crystallite sizes of $(\gamma MnO_2)_R$ and $(\gamma MnO_2)_L$ are similar. To complement the characterization of the electrode surface, energy dispersive of the two samples $(\gamma MnO_2)_R$ and $(\gamma MnO_2)_L$ were made. Besides magnesium, the presence of oxygen is also observed in the spectra as shown in Figs. 2a, 2b. In the EDX spectra of Fig. 2a, it is also possible to see the presence of sulphur (S) derived from the deposition solution. The SEM images shown in Figs. 2c, 2d indicate that the $(\gamma MnO_2)_R$ and $(\gamma MnO_2)_L$ products were ground to a smaller grain size and that the grain size distribution was more uniform.

Thermal Behavior

The general reaction scheme for the thermal treatment of γMnO_2 can be summarized as follows:

$$\gamma MnO_2 \rightarrow \beta MnO_2 \rightarrow Mn_2O_3.$$

As shown in Fig. 3, the first step where temperature is located between 100 and 450°C corresponds to the loss of water, as well as to a phase transition from the intergrowth γMnO_2 phase to the thermodynamically favored βMnO_2 phase. Three classes of water were found [24], the first one is physisorbed water, which is able to be reversibly and can be removed around 100°C. The second type of water is comprised at the surface bound hydroxyls and

Table 1. Lattice parameters *a*, *b*, and *c*, grain size *D* of $(\gamma MnO_2)_R$ and $(\gamma MnO_2)_L$ samples

Samples	*a,* nm	*b,* nm	*c,* nm	*D,* nm
$(\gamma MnO_2)_L$	1.1624	0.4204	0.2930	8
$(\gamma MnO_2)_R$	1.0522	0.4440	0.2479	6

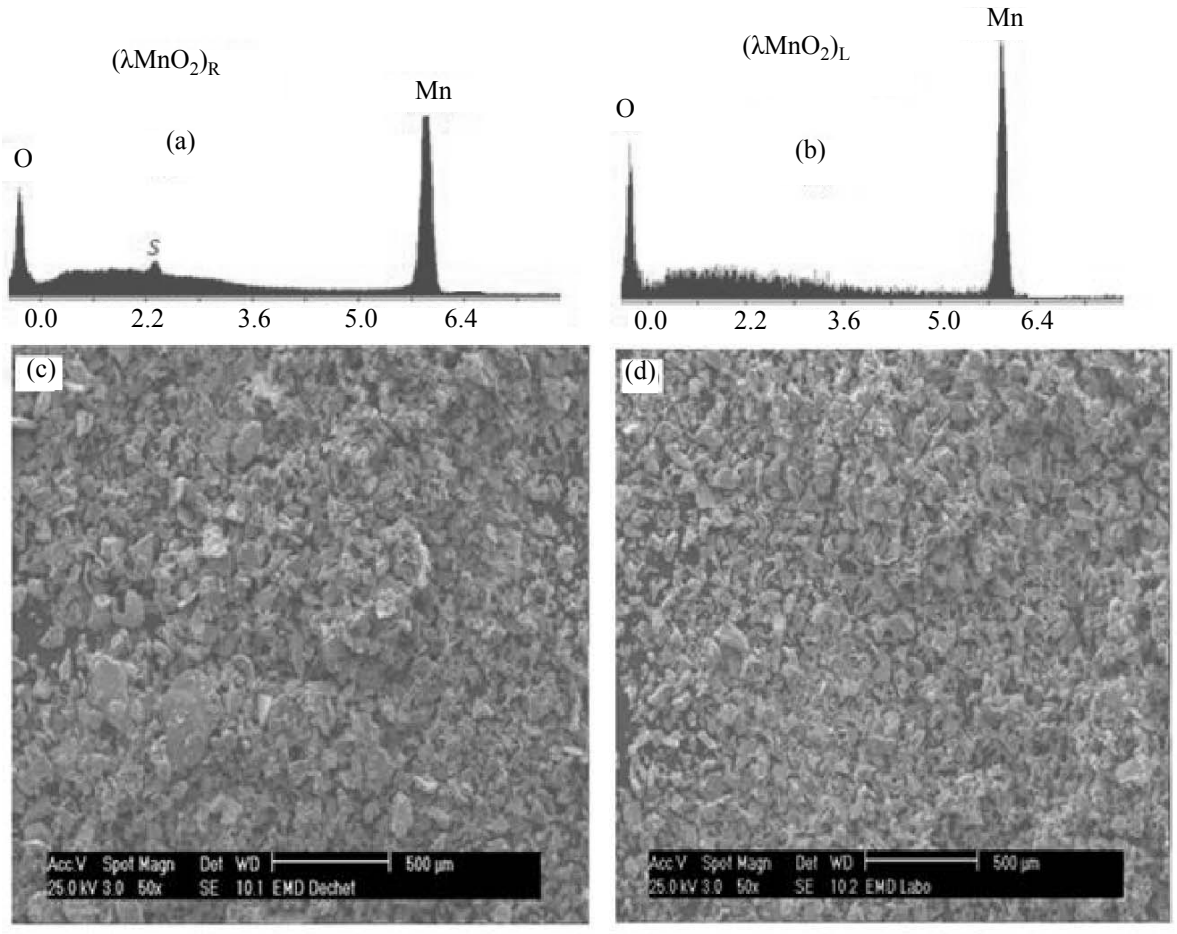

Fig. 2. EDX and SEM spectra for $(\gamma MnO_2)_R$ and $(\gamma MnO_2)_L$ samples.

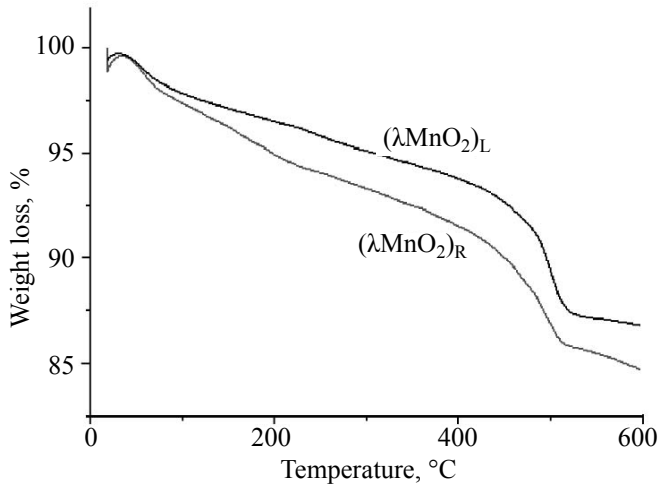

Fig. 3. TG curves of $(\gamma MnO_2)_R$ and $(\gamma MnO_2)_L$ samples.

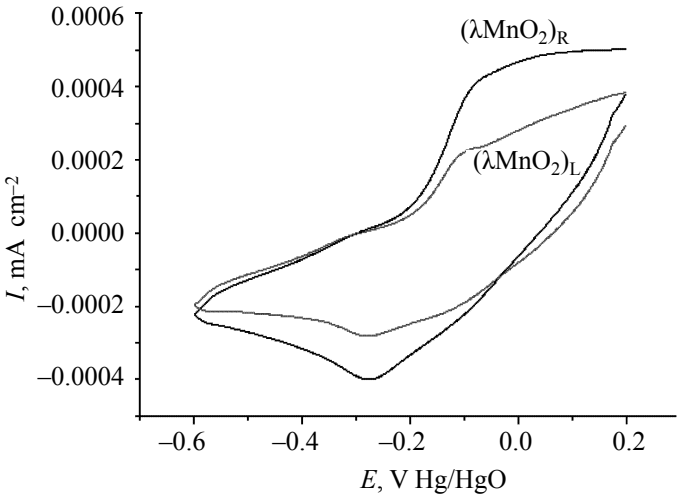

Fig. 4. Cyclic voltammograms for γMnO_2 scan rate 5 mV/s in 1 M [KOH].

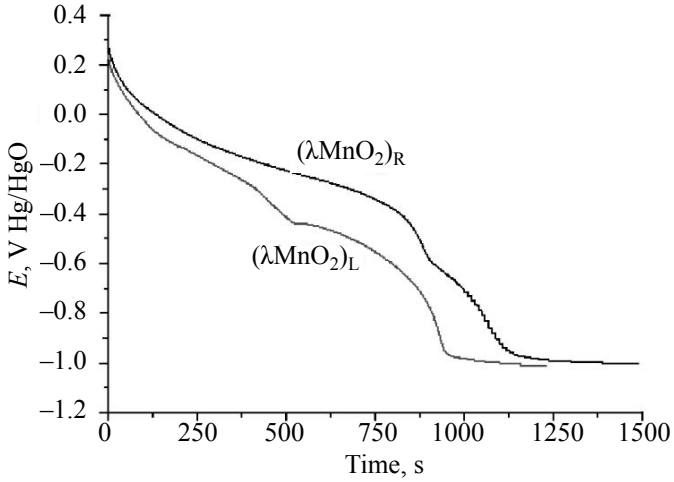

Fig. 5. Galvanostatic discharge curves obtained at cathodic current of 30 μA.

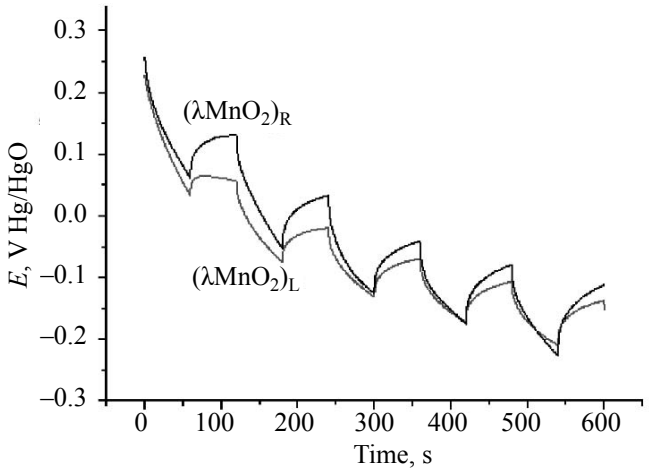

Fig. 6. Galvanostatic intermittent titration curves for both samples, at cathodic current 50 μA.

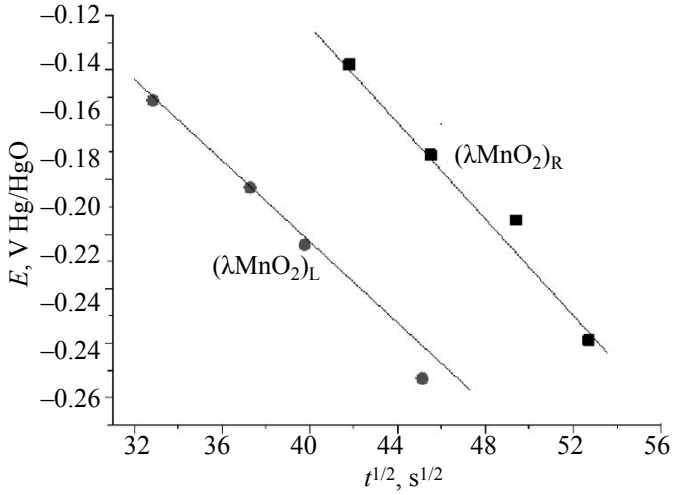

Fig. 7. Curves represents the variation of the potential with $\sqrt{t}$.

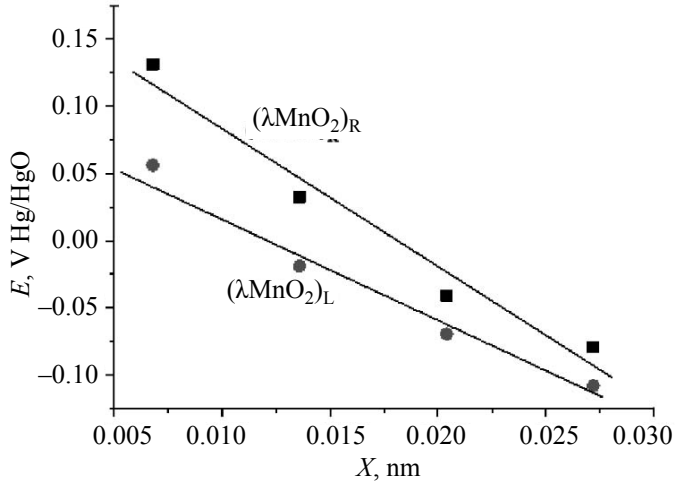

Fig. 8. Curves represents the variation of the potential $E_{i=0}$ with x.

are irreversibly removed around 200°C. The later one is a bulk hydroxyl group removed irreversibly at 300°C. Above 400°C, this step occurs in the range 400–600°C and corresponds to the training of the other oxides. Both curves of Fig. 3 are similar, thus we conclude that these samples exhibit the same thermal behavior.

Electrochemical Properties

Cyclic voltammetry. Figure 4 represents respectively the cyclic voltamogramms of the two samples. The curves show a large cathodic peak at −0.2 V followed by an anodic peak at −0.1 V vs. Hg/HgO. The cathodic peak corresponds to the reduction of MnO_2 to MnOOH and the anodic peak is relative to the oxidation of MnOOH to MnO_2.

Galvanostatic discharge. Figure 5 presented the galvanostatic discharge curves obtained at a cathodic current of 30 μA respectively for $(\gamma MnO_2)_R$ and $(\gamma MnO_2)_L$. Each curve presents two distinct plateaus. The first appears in the potential range 0.2 to −0.4 V Hg/HgO and corresponds to the reduction of MnO_2 to MnOOH, whereas, the second is located between −0.5 to −1 V Hg/HgO, which is relative to the conversion of MnOOH to $Mn(OH)_2$. $(\gamma MnO_2)_R$ shows a longer discharge time than $(\gamma MnO_2)_L$. The voltage started at above 0.2 V and decreased rapidly in $(\gamma MnO_2)_L$ case and reaches the value of −0.95 V during about 900 s.

Estimation of proton diffusion coefficient. In Fig. 6 we represent the galvanostatic intermittent titration curves for both samples. Initially samples are at equilibrium.

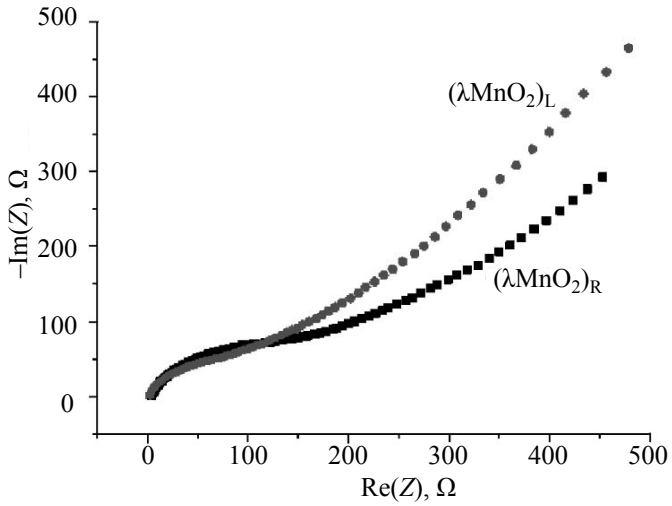

Fig. 9. Nyquist diagrams of γMnO_2 from 100 mHz to 10 kHz.

Under the influence of a cathodic current during 1 min (load and unload), we notice a decrease of the potetentiel of MnO_2.

From this spectra, we take four points which correspond to the intersection load-unload. We represent the variation of the potential according to the square root of time for $(\gamma MnO_2)_R$ and $(\gamma MnO_2)_L$ at a constant current of 30 μA as plotted in Fig. 7. These data were fitted linearly and on deduced the slope

$$dE/d[(t)^{1/2}] \text{ of the curve } E = f(t)^{1/2}.$$

On plotted also in Fig. 8 the variation of potential as a function of the injected hydrogen quantity x for $(\gamma MnO_2)_R$ and $(\gamma MnO_2)_L$ samples discharged at a constant current of 50 μA and 30 μA. This term x is the ratio between practical and theoretical capacity. On obtain a monotonous decrease of the potential when the x quantity is enhanced. The slope of this curve give the term $[(dE_i = 0)/dx]$. The different values of D were calculated from the following equation:

Table 2. Calculated proton diffusion coefficient of $(\gamma MnO_2)_R$ and $(\gamma MnO_2)_L$ samples

Samples	dE/dx, V mol^{-1}	dE, V s^{-1}	D_{H+}, cm^2 s^{-1}
$(\gamma MnO_2)_L$	−13.04	-8.43×10^{-3}	0.98×10^{-9}
$(\gamma MnO_2)_R$	−10.77	-6.14×10^{-3}	1.26×10^{-9}

$$D = [(2IV_M/F\pi^{1/2})(dE_{i=0}/dx)/(dE_{i=0}/dt^{1/2})]^2/S^2, \quad (3)$$

where S, D, I, V_M, F, $dE_{i=0}/dx$, $dE_{i=0}/dt^{1/2}$), x are espectively the geometric area of the working electrode, the proton diffusion coefficient, the current intensity, the molar volume of MnO_2, the Faraday's constant, slope of the curve $E = f(x)$, the slope of the curve $E = f(\sqrt{t})$ and x the quantity of hydrogen injected in MnO_2 by percent.

The calculated values of proton diffusion coefficient D are summarized in Table 2. From these results we can see that the D values calculated for $(\gamma MnO_2)_R$ and $(\gamma MnO_2)_L$ have the same order of magnitude, and this indicate that the electrolytic reactivity in both samples is almost the same.

Calculation of charge transfer resistance. Figure 9 represents the Niquist plots recorded at open circuit potential for $(\gamma MnO_2)_R$ and $(\gamma MnO_2)_L$. It represents the evolution of the imaginary part as a function of the real part to the impedance. On observed a monotonous parabolic increase in the imaginary part when the real part increases. The values of the charge transfer resistance (R_{ct}) deduced from the impedance plots of Fig. 7 for $(\gamma MnO_2)_R$ and $(\gamma MnO_2)_L$ are respectively 186.3 and 153.1 Ω. The data show that the (R_{ct}) values are similar. A semicircle which corresponds to the load resistance of transfer followed by a line which corresponds to Warburg diffusion.

CONCLUSIONS

The electrochemical behavior of MnO_2, using electrolysis of manganese sulfate solution recovered from used batteries and MnO_2 prepared from a commercial manganese sulfate solution, is studied in alkaline solution. The X-ray diffraction analysis show the same phase indexed as γMnO_2. We calculated the lattice parameters values of $(\gamma MnO_2)_R$ and $(\gamma MnO_2)_L$ for different crystallographic orientations. The analysis of SEM indicate that the $(\gamma MnO_2)_R$ and $(\gamma MnO_2)_L$ products have a smaller grain size, with an uniform distribution on surface. The two samples exhibit the same thermal profile with almost the same values of water content. The electrochemical investigation of the two samples gave a discharge capacity values more or less equal, with proton diffusion coefficient almost similar. In the light of these results, we conclude that MnO_2 could be synthesized at industrial scale from manganese sulfate solution recovered from used batteries. The charge transfer resistance deduced from the impedance plots for $(\gamma MnO_2)_R$ and $(\gamma MnO_2)_L$ were calculated.

REFERENCES

1. De Michelis. I , Ferella, F ,, Karakaya, E , Beolchini, F , and Veglió, F., *J. Power Sources,* vol. 172, pp. 975–983.
2. Nan, J., Han, D., Yang, M., Cui, M., and Hou, X., *Hydrometallurgy*, 2006, vol. 84, pp. 75–80.
3. Zhang, P., Yokoyama, T., Itabashi, O., Wakui. Y., Suzuki, T.M., and Inoque, K., *J. Power Sources,* 1999, vol. 77, pp. 116–122.
4. Muller, T. and Friedrich, B., *J. Power Sources*, 2006, vol. 158, pp. 1498–1509.
5. Li, L., Ge, J., and Wu, F., *J. Hazard. Mater*., 2006, vol. 176, pp. 288–293.
6. Shin, S.M, Kim, N.H, and Sohn, J.S., *Hydrometallurgy*, 2005, vol. 79, pp. 172–181.
7. Zhang. P.W., Yokoyama, T., and Itabashi, O., *Hydrometallurgy*, 1998, vol. 47, pp. 259–271.
8. Mantuano, D.P., Dorella, G., and Dorella. R.A., *J. Power Sources*, 2006, vol. 159, pp. 1510–1518.
9. Swain, B., Jeong, J., and Lee, J.C., *J. Power Sources,* 2007, vol. 167, pp. 536–544.
10. Freitas, M.B.J.G., Garcia, E.M., and Celante, V.G., *J. Appl. Electrochem.*, 2009, vol. 39, pp. 601– 607.
11. Garcia, E.M., Taroco, H.A., and Matencio, T., *J. Appl. Electrochem*., 2012, vol. 42, pp. 361– 366.
12. Garcia, E.M., Santos, J.S., and Pereira, E.C., *J. Power Sources,* 2008, vol. 185, pp. 549–553.
13. Bodoardo, S., Penazzi, N., Spinelli, P., and Arrabito, M., *J. Power Sources*, 2001, vol. 94, p. 194.
14. Sahoo, R.N., Naik, P.K., and Das, S.C., *Hydrometallurgy*, 2001, vol. 62, pp. 157–163
15. Perez–Benito, J.F., Arias, C., and Amata, E., *J. Colloid Interf. Sci.,* 1996, vol. 177, pp. 288–297.
16. Salgado, A.L., Veloso, A.M.O., Pereira, D.D., Gontijo, G.S., Salum, A., and Mansur, M.B., *J. Power Sources,* 2003, vol. 115, p. 367.
17. Jozwiak. P, Garbarczyk. J, Mauger. A, Gendron.F, and Julien. C., *J. Non–Cryst. Solids*, 2008354, p. 1915.
18. Kahil, H., Tejard, F., and Guitton, J., *Nuclear Sur. Techn.*, 1982, vol. 16, pp. 331–340.
19. Dwight, K. and Menyuk, N., *Phys. Rev.,* 1960, vol. 119, p. 1470.
20. Salgado, A.L, Veloso, A.M.O, Pereira, D.D, Gontijo, G.S, Salum., A, and Mansur, M.B., *J. Power Sources*, vol. 115, pp. 367–373.
21. Wu, B.L, Lincot, D., Vedel, J., and Yu, L.T., *J. Electroanal. Chem.*, 1997, vol. 420, pp. 159–165.
22. Fong, C., Kennedy, B.J., and Elcombe, M.M., *Zeitschrift fur Kristallographie*, 1994, vol. 209, pp. 941–945
23. Eberhart, J.P., *Analyse Structurale et Chimiques des Matériaux*, Bordas, Paris, 1989.
24. Dose, W.M. and Donne, S.W., *Mat. Sci. & Eng. B*, vol. 176, pp. 1169–1177.